

Squeeze dispersion and the effective diapycnal diffusivity of oceanic tracers

Note: We have simplified the title.

Gregory L Wagner ¹, **Glenn Flierl** ¹, **Raffaele Ferrari** ¹, **Gunnar Voet** ², **Glenn S Carter**
³, **Matthew H Alford** ², and **James B Girton** ⁴

⁶Earth, Atmospheric, and Planetary Sciences, Massachusetts Institute of Technology, Cambridge, MA

⁷Scripps Institution of Oceanography, University of California, San Diego, La Jolla, CA

⁸Department of Oceanography, University of Hawai'i at Manoa, Honolulu, HI

⁹Applied Physics Laboratory, University of Washington, Seattle, WA

Key Points:

- Squeezing and stretching of density layers modulates the diapycnal diffusion of oceanic tracers
- Squeeze dispersion modulates dispersion across some isopycnals in the abyssal Samoan Passage
- Diapycnal transport is strongly affected by positive correlations between squeezing and turbulence

17 **Abstract**

18 We describe a process called ‘squeeze dispersion’ in which the squeezing of oceanic tracer
 19 gradients by waves, eddies, and bathymetric flow modulates diapycnal fluxes by centime-
 20 ter to meter-scale turbulence. Due to squeeze dispersion, the average effective diapycnal
 21 diffusivity of oceanic tracers is different and typically greater than the average ‘local’ dif-
 22 fusivity, especially when local diffusivity correlates with squeezing. We develop a theory to
 23 quantify the effects of squeeze dispersion on diapycnal oceanic transport, finding formu-
 24 las that connect density-average tracer flux, locally-measured diffusivity, large-scale oceanic
 25 strain, the thickness-weighted average buoyancy gradient, and the effective diffusivity of
 26 oceanic tracers. We use this effective diffusivity to interpret observations of abyssal flow
 27 through the Samoan Passage reported by Alford et al. (2013) and find that squeezing mod-
 28 ulates diapycnal tracer dispersion by factors between 0.5 and 3.

29 **Plain language summary**

30 Turbulent vertical ocean mixing is a crucial part of the Earth’s climate system, drawing drawing
 31 atmospheric carbon and heat into the massive reservoir that is the deep ocean. Quan-
 32 tifying vertical ocean mixing is difficult: vertical mixing is associated with turbulence at the
 33 tiny scales of centimeters to meters, but affects the entire ocean on the long time scales
 34 of decades and centuries. We demonstrate that vertical ocean mixing depends not *only* on
 35 small scale turbulence as previously thought, but on the *combination* of small scale turbu-
 36 lence and larger scale motions, such as currents, eddies and waves similar to the jet streams
 37 and hurricanes of the atmosphere. In particular, when a patch of ocean is mixed by small-
 38 scale turbulence while being ‘squeezed’ in the vertical at the same time by currents and ed-
 39 dyes, the patch ultimately mixes more quickly than the turbulence would cause alone. This
 40 means that estimating the total rate of oceanic vertical mixing requires knowledge both of
 41 the magnitude of ocean squeezing as well as the intensity of small scale ocean turbulence.

42

43 **1 Introduction**

44 *Note: We have made small changes to the first few paragraphs of the introduction and the*
 45 *mathematical notation in our toy example to clarify and enhance our explanation of the basic mech-*
 46 *anism of squeeze dispersion and the scenarios in which it is relevant.*

47 Squeeze dispersion is a process in which the diapycnal diffusion of tracers such as dis-
 48 solved carbon, temperature, salinity, oxygen, nutrients, and plankton is modulated in fluc-
 49 tuating flows that alternately squeeze material surfaces together and stretch them apart.
 50 Squeeze dispersion is a non-turbulent process relevant to flows that have moderate strain,
 51 but lack the crinkling, rolling up, and exponential stretching of material surfaces associated
 52 with turbulent mixing. Squeeze dispersion plays a role in flows under strong geometric or
 53 dynamical constraints: for example, low Reynolds flows confined by solid boundaries, or strat-
 54 ified, rotating, and anisotropic planetary flows.

55 In this paper we explore the effect of squeeze dispersion on transport across density
 56 surfaces in Earth’s ocean, where strong stratification and rotation limits turbulent mixing
 57 to ‘microscales’ smaller than approximately ten meters. Where a wide scale separation be-
 58 tween microscale mixing and ‘macroscale’ flows with vertical scales of ten to thousands of
 59 meters exists, diapycnal fluxes are, from perspective of macroscale flows, approximately dif-
 60 fusive and characterized by an inhomogeneous and isotropic local diffusivity, κ . Macroscale
 61 flows associated with strain and squeeze dispersion include mesoscale and submesoscale
 62 eddies, fronts, and large-scale internal waves.

63 An estimate for the vertical diffusive flux across a squeezed macroscale layer of fluid
 64 illustrates the basic mechanism of squeeze dispersion. In this scenario, depicted in figure 1,
 65 a layer of fluid bound between material and isotracer surfaces with concentrations c and
 66 $c + \Delta c$ is squeezed and stretched by a macroscale flow with strain but no overturning. Mi-
 67 croscale turbulent mixing across the layer associated with overturning on scales much smaller
 68 than the separation between the two surfaces is characterized by the vertical diffusive flux
 69 $F = -\kappa \Delta c / h$, where κ is the isotropic turbulent diffusivity and h is the vertical separa-
 70 tion between the surfaces.

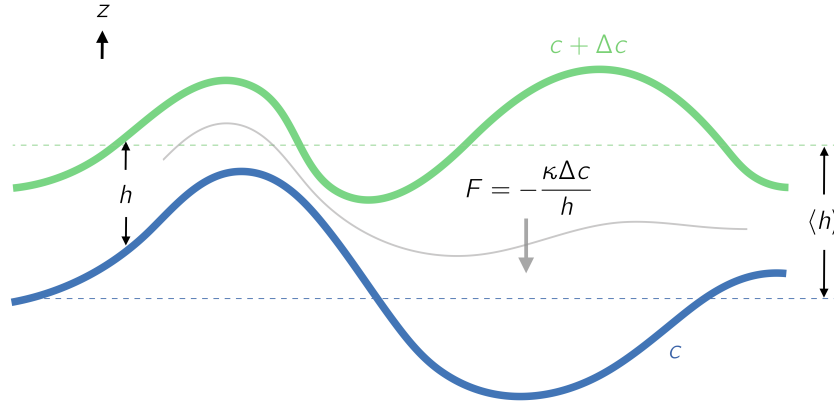


Figure 1: Squeeze dispersion between two isotracer surfaces with tracer concentrations c and $c + \Delta c$. The diffusive flux between the fluctuating surfaces is $F = -\kappa \Delta c / h$, where h is the separation between the surfaces and κ is the local diffusivity across the layer. The spatially-averaged separation between the two surfaces is $\langle h \rangle$. Introducing an effective squeeze dispersion diffusivity $\kappa_e = \langle h \rangle \langle \kappa / h \rangle$ implies that $\langle F \rangle = -\kappa_e \Delta c / \langle h \rangle$.

The average vertical tracer flux across the layer is $\langle F \rangle = -\Delta c \langle \kappa / h \rangle$, where the angle brackets denote an average that follows the motion of the layer and encompasses fluctuations in both h and κ . This formula for $\langle F \rangle$ reflects the intuitive fact that, relative to a fixed κ distribution, an increase in squeezing and thus variations in h acts to increase the average flux $\langle F \rangle$ across the layer. Increasing diffusive flux with increasing strain is the hallmark of squeeze dispersion. To express $\langle F \rangle$ in terms of the average separation between the surfaces $\langle h \rangle$ we introduce the effective diffusivity,

$$\kappa_e = \langle h \rangle \left\langle \frac{\kappa}{h} \right\rangle, \quad (1)$$

such that $\langle F \rangle = -\kappa_e \Delta c / \langle h \rangle$.

Note: In response to reviewer 1's first comment, we have added the following paragraph to emphasize our focus on the process of squeeze dispersion, rather than the particular quantification of its effect using a particular average.

The squeeze dispersion effective diffusivity in (1) is simple quantification of the effects of the squeeze dispersion process that depends on an average that follows the vertical motion of a strained layer of fluid. The squeeze dispersion process itself does not, however, depend on the averaging method — Lagrangian, Eulerian, or otherwise — used to quantify its effect. To make this point concrete, we introduce an example in section 2 that illustrates squeeze dispersion in the advection of a tracer patch over undulating bathymetry by a spatially-variable, squeezing and stretching barotropic flow. In this example, the effective diffusivity in (1) arises in the exact analytical solution to the barotropic squeezing

problem. In section 3, we show further that the effective diffusivity (1) arises in the thickness-weighted-average equation (9) for the dispersion of tracers on the scales of ocean circulation alongside the familiar processes of advection by the residual-mean circulating velocity and isopycnal diffusive mixing by mesoscale eddies.

The effective diffusivity (1) is a bulk diffusivity obtained by averaging tracer flux over macroscale fluctuations and along isopycnals and dividing the result by the thickness-weighted-average tracer gradient. This interpretation of (1) in terms of tracer fluxes suggests a method for analyzing microstructure observations that makes use of Osborn (1980)'s hypothesized relationship between turbulent dissipation rate and buoyancy flux: rather than 'averaging κ ', the computation of (1) requires averaging the buoyancy flux $\Gamma\epsilon$ along surfaces or layers of constant density, where Γ is the mixing coefficient, the proportionality constant between turbulent dissipation rate ϵ and local buoyancy flux.

In section 4, we implement this method for calculating κ_e in (1) in an analysis of microstructure observations from the Samoan Passage, and find that the effective diapycnal diffusivity of tracers advected through the Samoan passage differs from the isopycnal-averaged local diffusivity by factors of 0.5–3. This difference between bulk effective diffusivity and average local diffusivity in the Samoan passage suggests that realistic variations in diffusivity and squeezing can cause substantial modulation in the dispersion of oceanic tracers. The difference between average diffusivity and effective squeeze dispersion diffusivity may contribute to differences between tracer-based and microstructure-based estimates of diapycnal diffusivity inferred from observations as, for example, in the Brazil Basin (Ledwell et al., 2000), the east Pacific sector of the Antarctic Circumpolar Current (Ledwell, St. Laurent, Girton, & Toole, 2011), and Drake Passage (Mashayek et al., 2017; St. Laurent et al., 2012; Watson et al., 2013).

2 Squeeze dispersion in flow over undulating bathymetry

The squeeze dispersion process is illustrated by the advection of a diffusing tracer patch through the contracting streamlines of a two-dimensional flow $u(x), w(x, z)$. This example may be alternatively interpreted as mid-depth tracer dispersion in a barotropic shallow water flow with rigid lid and undulating bathymetry, or as the advection of a tracer patch between two isopycnals in a slowly-varying, large-scale straining flow.

In either interpretation, the effects of microscale turbulent mixing are modeled by an inhomogeneous turbulent diffusivity, $\kappa(x, z, t)$. The tracer concentration $c(x, z, t)$ then obeys the advection-diffusion equation

$$c_t + uc_x + wc_z = \partial_x(\kappa c_x) + \partial_z(\kappa c_z), \quad (2)$$

where the barotropic horizontal and vertical velocity are

$$u(x) = \frac{U}{H} \quad \text{and} \quad w(x, z) = \frac{zUH_x}{H^2}, \quad (3)$$

with barotropic transport U , length L , depth

$$H(x) = \langle H \rangle [1 - a \sin(\frac{2\pi x}{L})], \quad (4)$$

average depth $\langle H \rangle$, and non-dimensional relative bathymetric height a .

Figure 2(a) shows a time lapse of the evolution of an initially Gaussian tracer patch with $\int c dx dz = 1$ squeezed and stretched by the flow in (3) with constant κ . We compare the prescribed κ to the measured effective diffusivity $\kappa_e = (2T)^{-1} \int (Z-z)^2 c dx dz$, where $Z = \int z c dx dz$ is the z-centroid of the tracer patch, based on the change in the vertical variance of the tracer patch over the interval $T = \langle H \rangle L/U$ during which the patch

travels from $x = 0$ to $x = L$. This definition of κ_e , introduced by Aris (1956), is used to interpret oceanic tracer release experiments such as that reported by Ledwell et al. (2011). In figure 2(b), the ratio between the numerically measured effective diffusivity κ_e and the prescribed constant diffusivity κ is plotted with purple circles, showing how squeeze dispersion always increases κ_e over a constant κ . This is squeeze dispersion: tracer dispersion increases with increasing a and thus increasing squeezing, despite acceleration of the tracer patch over the constriction and stretching over the contraction.

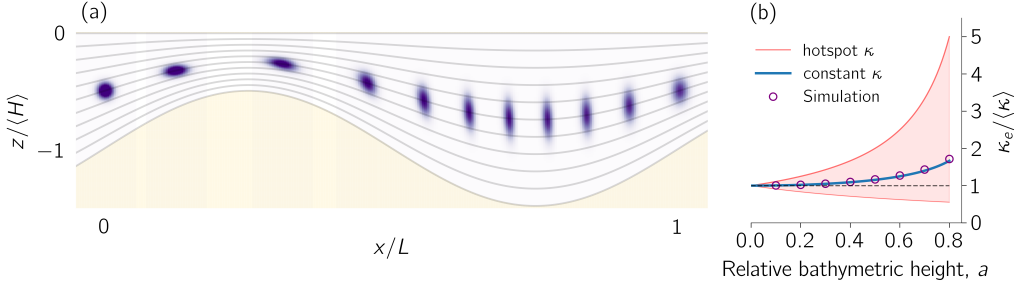


Figure 2: (a) Time-lapse of tracer patch advection in a numerical solution to (2)–(4) with $a = 0.5$. (b) Modulation of diffusion by squeeze dispersion in a numerical solution to (2)–(4) (purple circles) with constant κ , the theoretical prediction 6 with constant κ (blue line), and the theoretical prediction for mixing ‘hotspots’ located at the point of maximum squeezing ($\kappa \propto \delta(x + L/4)$, upper red line) and the point of maximum stretching ($\kappa \propto \delta(x + 3L/4)$, lower red line). Red shading indicates the range of possible modulation of diffusion by squeezing in this problem and a grey dashed line indicates $\kappa_e / \langle \kappa \rangle = 1$. We use $U = 1$, $\langle H \rangle = 1$, $L = 20$, $\kappa = 10^{-4} \text{ m}^2 \text{ s}^{-1}$ and tracer initial condition $c(t = 0) = \exp[-x^2/2\ell^2 - (z + \langle H \rangle/2)^2/2d^2]/2\pi\ell d$ with $\ell = L/100$ and $d = \langle H \rangle/20$. Note: We have improved figure 2 to emphasize the streamlines in 2(a), and have included theoretical calculations of dispersion ‘maximization’ and ‘minimization’ in 2(b) due to hotspots located in regions of squeezing or stretching.

The nature of this enhancement in dispersion is revealed by a special solution to (2)–(3) derived in appendix A in which we assume the tracer patch has a thin aspect ratio such that $\partial_x(\kappa c_x) \ll \partial_z(\kappa c_z)$, use a transformation into bathymetric coordinates with the initial condition $c(t = 0) = \delta(x)\delta(z + \langle H \rangle/2)$, and allow turbulent diffusivities of the form $\kappa(x, t)$. The tracer distribution in this solution is tellingly Gaussian after being advected for a time $t_n = n\langle H \rangle L/U$ through n ‘squeezing cycles’ over the periodic bathymetry,

$$c(t = t_n) = \frac{1}{\sqrt{4\pi\kappa_e t_n}} \exp\left[-\frac{(z + \langle H \rangle/2)^2}{4\kappa_e t_n}\right] \delta(x - nL), \quad (5)$$

and therefore spreads diffusively in the vertical while advected horizontally. However, rather than spreading with the trajectory-averaged diffusivity, for example, the effective diffusivity that determines tracer patch dispersion is

$$\kappa_e = \langle H \rangle \left\langle \frac{\kappa}{H} \right\rangle, \quad \text{where} \quad \langle \phi \rangle \stackrel{\text{def}}{=} \frac{1}{L} \int_0^L \phi \, dx. \quad (6)$$

κ_e in (5)–(6) is identical to the effective diffusivity defined in terms of the growth of tracer variance, $\kappa_e = (2T)^{-1} \int (Z - z)^2 c \, dx dz$. Because $\langle 1/H \rangle \geq 1/\langle H \rangle$ for any positive function $H(x)$, (6) implies that fluctuating squeezing always enhances the diffusive transport

129 associated with a constant κ . Moreover, the enhancement is increased further relative to
 130 $\langle \kappa \rangle$ when κ and squeezing positively correlate.

131 In figure 2(b) we compare the diffusivity modulation $\kappa_e / \langle \kappa \rangle$ in numerical solutions
 132 to (2) (purple circles) with the theoretical prediction (6) (blue line) versus a . The numer-
 133 ical and analytical solutions show that $\kappa_e / \langle \kappa \rangle > 1$ for constant κ , corresponding to a mod-
 134 est enhancement in tracer diffusion due to squeeze dispersion. The slight disagreement be-
 135 tween the numerical and analytical solutions for constant κ is due to the contribution of
 136 horizontal diffusion and shear to the vertical dispersion of the patch in the numerical so-
 137 lution. The red solid lines plot (6) for diffusivity ‘hot spots’ associated with $\kappa \propto \delta(x -$
 138 $L/4)$ (upper red line) and $\kappa \propto \delta(x - 3L/4)$ (lower red line) that form upper and lower
 139 bounds for the modulation of κ_e due to squeeze dispersion, showing how correlations be-
 140 tween squeezing and a non-constant κ can act to either reduce or significantly enhance the
 141 tracer effective diffusivity κ_e relative to $\langle \kappa \rangle$.

142 3 Effect of squeeze dispersion on the circulation of oceanic tracers

143 In this section we show that squeeze dispersion affects the diapycnal diffusion of trac-
 144 ers on the scales of ocean circulation in continuous, depth-dependent stratification and flow.
 145 For this we use a series of two averages introduced by both De Szoeke and Bennett (1993)
 146 and Young (2012) to obtain a description of circulation-scale oceanic tracers that distin-
 147 guishes between advection by the residual-mean circulation, isopycnal dispersion by mesoscale
 148 eddies, and diapycnal squeeze dispersion by microstructure turbulence.

We first apply a spatial ‘microscale average’ over turbulent fluctuations and density inversions on scales of centimeters to $O(10)$ meters. The microscale average (*i*) yields a monotonic density field and enables the use of buoyancy coordinates, and (*ii*) permits the turbulent closure $\tilde{\mathbf{u}}\tilde{c} = -\kappa\nabla c$ for the average microscale turbulent flux $\tilde{\mathbf{u}}\tilde{c}$, where $\tilde{\mathbf{u}}$ is the microscale velocity field, \tilde{c} is the microscale tracer concentration, κ is the microscale turbulent diffusivity and ∇c is the ‘macroscale’ tracer gradient. The macroscale tracer concentration c then obeys

$$c_t + \mathbf{u} \cdot \nabla c = \nabla \cdot (\kappa \nabla c), \quad (7)$$

149 where the advecting velocity field \mathbf{u} includes large scale internal waves as well as subme-
 150 soscale, quasi-geostrophic, and bathymetric flows with vertical scales larger than 10 me-
 151 ters.

We introduce a second, thickness-weighted ‘macroscale average’ defined for any variable ϕ via

$$\hat{\phi} \stackrel{\text{def}}{=} \frac{\langle h\phi \rangle}{\langle h \rangle}. \quad (8)$$

152 In (8), $h \stackrel{\text{def}}{=} g/b_z$ is the ‘thickness’ of the buoyancy surface $b = -gp'/\rho_0$, where g is grav-
 153 itational acceleration, ρ_0 is a reference potential density, and p' is the potential density per-
 154 turbation therefrom. The angle brackets in (8) denote an ensemble, time, or spatial av-
 155 erage over macroscale fluctuations in buoyancy coordinates (Young, 2012). Though our
 156 results are strictly true only for ensemble averages, time or spatial averages may be used
 157 to similar but approximate effect where ensembles of oceanic motion are not available (Davis,
 158 1994). Averaging in buoyancy coordinates is crucial for distinguishing between fundamen-
 159 tal circulation processes: advection of tracer by the residual velocity, stirring of tracers along
 160 mean isopycnal surfaces by mesoscale eddies, and mixing across mean density surfaces by
 161 microscale turbulence.

We show in appendix B that applying the thickness-weighted average in (8) to the macroscale tracer equation (7) leads to an equation for the evolution of tracers on the scales

of ocean circulation:

$$\left(\partial_t + \mathbf{u}^\# \cdot \nabla - \partial_z \langle h \rangle \underbrace{\left\langle \frac{\kappa}{h} \right\rangle}_{\stackrel{\text{def}}{=} \kappa_e} \partial_z \right) \hat{c} = -\nabla \cdot \mathbf{E}^c. \quad (9)$$

Equation (9) describes the dispersion of the large-scale tracer concentration \hat{c} due to advection by the circulation velocity $\mathbf{u}^\#$, stirring and diffusion by macroscale eddy fluxes \mathbf{E}^c defined in (B.14), and across-isopycnal diffusion due to the effective diapycnal diffusivity $\kappa_e = \langle h \rangle \langle \kappa/h \rangle$.

Note: We have updated the following paragraph to address reviewer 1's concerns and correct our mischaracterization of the Gent-McWilliams scheme as a parameterization of the bolus velocity.

Ocean models that employ the Gent and Mcwilliams (1990) scheme to parameterize mean advection by mesoscale eddies and the Redi diffusivity (Redi, 1982) to parameterize eddy mixing along isopycnals may implicitly use (9) to model the dispersion of oceanic tracers (McDougall & Mcintosh, 2001). In these models, the Redi diffusivity acts to parameterize the eddy fluxes \mathbf{E}^c in (9), while the advecting velocity field $\mathbf{u}^\#$ is modeled as the sum of a resolved velocity field and a 'quasi-Stokes' velocity field (McDougall & Mcintosh, 2001) approximated by the Gent and Mcwilliams (1990) scheme. In these models and in actuality, isopycnal advection and mixing dominate the isopycnal dispersion of oceanic tracers at large scales. Equation (9) demonstrates how diapycnal squeeze dispersion complements isopycnal mixing by eddy fluxes \mathbf{E}^c and residual advection by $\mathbf{u}^\#$ to determine the total — along-isopycnal and cross-isopycnal — dispersion of oceanic tracers.

The effective diapycnal diffusivity experienced by oceanic tracers is given by the squeeze dispersion formula $\kappa_e = \langle h \rangle \langle \kappa/h \rangle$, directly analogous to the effective diffusivity (6) that emerges in the parameterization in the introduction and the barotropic problem in section 2. The coarse-grained argument developed in the introduction thus translates to cases with continuous stratification and flow, in which advection by vertically convergent and divergent flows acts to increase and decrease vertical tracer gradients. The mediation of oceanic tracer diffusion by squeeze dispersion implies an outsized importance for correlations either dynamical or coincidental between squeezing and microscale turbulence.

4 Squeeze dispersion in the Samoan Passage

Note: We have significantly improved our analysis of the Samoan passage data. We now average buoyancy flux directly from the observations rather than backing out the average buoyancy flux from the local κ (which in the original manuscript was itself inferred from local buoyancy flux). The results plotted in figure 3 are not significantly changed in our new analysis. However, we believe this new method is more faithful to the original data, systematic, and careful than our previous method.

To evaluate the effect of squeeze dispersion in observed oceanic scenarios, we compare the effective squeeze diffusivity in (1) and (9) with the average local diffusivity of a hypothetical tracer advected along isopycnals in observations of abyssal flow through the Samoan Passage — a 40 km-wide conduit between the southern and northern Pacific Ocean where strong abyssal flow over rough and constricted bathymetry produces hydraulic jumps, lee waves, turbulence, and squeezing. We focus on the eastern channel of the Samoan Passage using a series of hydrographic and direct turbulence observations made in 2012 summarized in figure 3(a) and by Alford et al. (2013).

Our analysis uses 13 vertical profiles of small-scale shear, temperature, and pressure made by a Rockland Vertical Microstructure Profiler (VMP). The location of the 13 VMP

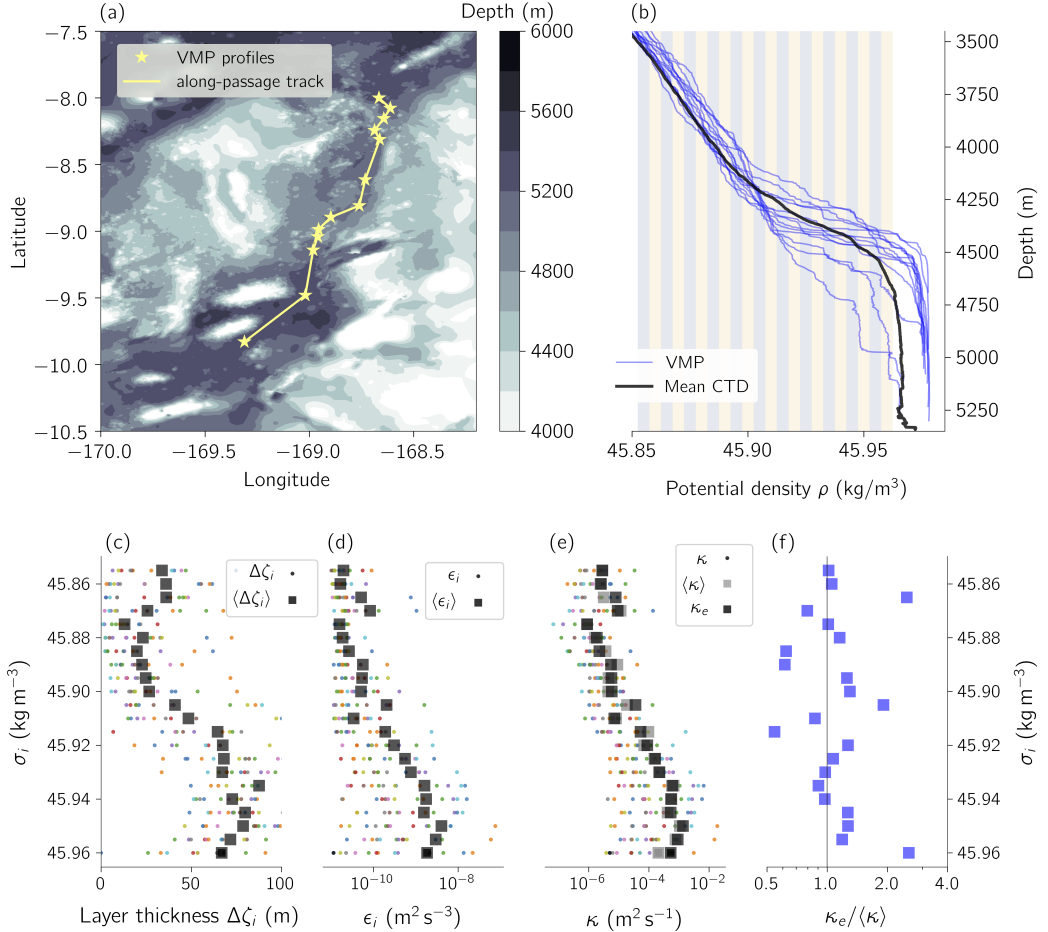


Figure 3: Effect of squeezing on diapycnal dispersion in the Samoan passage. (a) shows Samoan Passage bathymetry and VMP profile locations. (b) shows VMP density profiles in blue, the mean of 8 passage CTD density profiles in black, and the 22 density layers used for analysis with vertical stripes. (c), (d), and (e) show profiles and passage averages of layer thickness $\Delta\zeta_i$, layer-averaged turbulent dissipation rate ϵ_i , and cross-layer diffusivity κ_i . (e) also plots effective diffusivity κ_e and (f) plots the ratio $\kappa_e/\langle\kappa\rangle$. Note: We have added panel (d) to show the layer-averaged dissipation rate, ϵ_i .

205 profiles are overlain over contours of Samoan passage bathymetry in figure 3(a). Because
 206 conductivity was not measured by the VMP, we estimate VMP salinity with a 5th-order poly-
 207 nomial fit to the temperature-salinity relationship measured by nearby Sea-Bird 911plus Conductivity-
 208 Temperature-Depth (CTD) profiles. The temperature, conductivity, and pressure profiles
 209 are processed to produce 1 meter gridded data and used to compute profiles of potential
 210 density referenced to 4,000 meters, which we denote σ . The turbulent kinetic energy dis-
 211 sipation rate, $\epsilon \stackrel{\text{def}}{=} \nu |\nabla \tilde{u}|^2$, where ν is the kinematic ocean viscosity and \tilde{u} is the microscale
 212 velocity field, is estimated from the VMP data by fitting local shear fluctuation spectra to
 213 the Nasmyth spectrum (Oakey & Elliott, 1982) and further integrating following Gregg (1998).

214 We next define 22 layers equally distributed in density space between $\sigma = 45.85 \text{ kg m}^{-3}$
 215 and $\sigma = 45.96 \text{ kg m}^{-3}$ with width $\Delta\sigma = 0.005 \text{ kg m}^{-3}$. The depth of these 22 density
 216 layers ranges from 3144 to 5106 meters within the 13 VMP profiles. The gridded $\sigma(z)$ pro-
 217 files and 22 density layers $\sigma_i \pm \frac{1}{2}\Delta\sigma$ are visualized in figure (3)(b).

The vertical extent of each density layer, $\Delta\zeta_i$, and layer-averaged turbulent dissipa-
 tion, ϵ_i , are computed for each profile by sorting the σ profile to obtain a monotonic, sta-
 bly stratified density profile $\sigma'(z)$ and permuting ϵ to find ϵ' such that $\epsilon'(\sigma') = \epsilon(\sigma)$. We
 next invert $\sigma'(z)$ to find $\zeta' = z(\sigma')$, where z is a vertical coordinate that increases up-
 wards to $z = 0$ at the ocean surface, and linearly interpolate ζ' in σ' to determine $\Delta\zeta_i$ via

$$\Delta\zeta_i = \zeta'(\sigma_i - \frac{1}{2}\Delta\sigma) - \zeta'(\sigma_i + \frac{1}{2}\Delta\sigma). \quad (10)$$

We compute the layer-averaged dissipation, ϵ_i , from the sorted data by evaluating

$$\epsilon_i(\sigma_i) = \frac{1}{\Delta\sigma} \int_{\sigma_i - \Delta\sigma/2}^{\sigma_i + \Delta\sigma/2} \epsilon'(\sigma') d\sigma', \quad (11)$$

218 numerically with the trapezoidal rule and using linear interpolation in σ' to estimate ϵ' at
 219 the end points $\sigma_i \pm \frac{1}{2}\Delta\sigma$. Finally, we note that the maximum overturn density adjustment
 220 $\max(|\sigma' - \sigma|)$ over all profiles is 0.0014 kg m^{-3} , smaller than the layer size $\Delta\sigma = 0.005$.

We compute the local diffusivity across each density layer using Osborn (1980)'s for-
 mula for the relationship between turbulent dissipation and buoyancy flux,

$$\kappa(\sigma_i) \stackrel{\text{def}}{=} \frac{\Gamma \epsilon_i}{N_i^2}, \quad (12)$$

where $\Gamma = 0.2$ is the mixing coefficient, the ratio between potential energy creation and
 kinetic energy dissipation. In (12), N_i^2 is the buoyancy gradient across each σ_i layer defined
 in terms of $\Delta\zeta_i$ via

$$N_i^2 = -\frac{g\Delta\sigma}{\rho_0 \Delta\zeta_i}, \quad (13)$$

221 where $g = 9.81 \text{ m s}^{-2}$ is gravitational acceleration and $\rho_0 = 1045.85 \text{ kg m}^{-3}$. (The spe-
 222 cific values of g and ρ_0 are irrelevant to the main conclusions of this section based on the
 223 ratio between effective diffusivity and local diffusivity.)

We develop a bulk average by defining an along-passage track that connects the 13
 VMP stations with straight lines in latitude-longitude coordinates, and defining an along-
 passage coordinate 'x' that increases along the track from south to north. The along-passage
 track connecting VMP stations is shown in figure 3(a). We define an average of any vari-
 able $\phi(x, \sigma_i)$ within a density layer σ_i and along the Samoan passage as

$$\langle \phi \rangle(\sigma_i) \stackrel{\text{def}}{=} \frac{1}{L} \int_0^L \phi(x, \sigma_i) dx, \quad (14)$$

224 where x is distance on the along-passage track in figure 3(a) and L is the total length of
 225 path connecting the VMP profiles. The integral in (14) is estimated from the discrete data

226 using the trapezoidal rule. In Figure 3(c), (d), and (e), we compare the profiles and passage-
227 averages of $\Delta\zeta_i$, ϵ_i , and κ , respectively.

We use (14) to compute the effective diffusivity in (1) and (9), $\kappa_e = \langle h \rangle \langle \kappa/h \rangle$, where
the thickness is defined $h = g/N^2$ in terms of the local buoyancy gradient N^2 and grav-
itational acceleration g . This definition of the effective diffusivity with the average in (14)
is reminiscent of the definition that appears in the effective diffusivity derived for the barotropic,
'single-layer' example in section 2. Inserting the formula for local diffusivity κ in (12) into
the squeeze dispersion formula $\kappa_e = \langle h \rangle \langle \kappa/h \rangle$ yields

$$\kappa_e(\sigma_i) = \left\langle \frac{1}{N_i^2} \right\rangle \langle \Gamma \epsilon_i \rangle . \quad (15)$$

$$= -\frac{\rho_0}{g \Delta \sigma} \langle \Delta \zeta_i \rangle \langle \Gamma \epsilon_i \rangle . \quad (16)$$

The ratio between the passage-averaged effective diffusivity (16) and the average local dif-
fusivity,

$$\frac{\kappa_e}{\langle \kappa \rangle} = \frac{\langle \Delta \zeta_i \rangle \langle \epsilon_i \rangle}{\langle \Delta \zeta_i \epsilon_i \rangle} , \quad (17)$$

228 makes clear how substantial positive or negative correlations between turbulent mixing rep-
229 resented by ϵ_i and squeezing represented by $\Delta\zeta_i$ imply a substantial difference between tur-
230 bulent buoyancy flux and the associated effective diffusivity, and the average local diffusiv-
231 ity. In other words, $\kappa_e/\langle \kappa \rangle \geq 1$ implies a correlation between large ϵ_i (mixing) and small
232 $\Delta\zeta_i$ (squeezing).

233 The layerwise effective diffusivity in (16) and ratio $\kappa_e/\langle \kappa \rangle$ in (17) are plotted in fig-
234 ure 3(e) and (f). $\kappa_e/\langle \kappa \rangle$ varies from 0.5–3, and is greater than unity more often than not.
235 The substantial discrepancy between the isopycnal-averaged local diffusivity and the effec-
236 tive squeeze diffusivity across some isopycnals implies that strain substantially affects to-
237 tal tracer dispersion in the Samoan passage.

238 5 Conclusions

239 'Squeeze dispersion' is a process by which diapycnal strain modulates oceanic diapy-
240 cnal mixing. The importance of squeeze dispersion on net diapycnal mixing depends on (i)
241 the magnitude of oceanic vertical strain and squeezing and (ii) correlations between squeez-
242 ing and diapycnal turbulence. Squeezing is often weak in mesoscale oceanic flows, being
243 proportional to Rossby number in quasi-geostrophic flows or the nonlinearity of internal wave
244 fields. Yet plausible dynamical mechanisms may link mixing and strain: for example, squeez-
245 ing and intense turbulent mixing are co-located over mountainous bathymetry in the Samoan
246 Passage. Numerical simulations suggest that large-scale strain may enhance turbulent in-
247 tensity and mixing in preexisting shear layers (Kaminski, 2016). On the other hand, Alford
248 and Pinkel (2000) find a *negative* correlation between squeezing and turbulent overturns
249 and mixing in the near-surface ocean. Further observations and simulations are needed to
250 determine the relationship between oceanic strain and turbulent mixing throughout the wa-
251 ter column, especially where turbulence is strong and κ is large.

252 *Note: We have included the following paragraph to address reviewer 1's first comment about*
253 *the apparent absence of squeeze dispersion in an Eulerian-averaged analysis.*

254 In section 3 we conduct an analysis of the effects of squeeze dispersion on tracer fluxes
255 across isopycnal surfaces with the thickness-weighted average that culminates in an expres-
256 sion for the effective diffusivity of the thickness-weighted average tracer distribution in (9).
257 The effective diffusivity does not necessarily describe the evolution of other average tracer
258 distributions. Take the Eulerian-average, for example: the Eulerian-average tracer flux due
259 to squeeze dispersion may include contributions both from the modified Eulerian-average

260 diffusive tracer flux and the Eulerian-average advective flux. Both of these are proportional
 261 to κ in non-turbulent squeeze dispersion processes. In general, both the average tracer dis-
 262 tribution and its effective diffusivity depend on whether the average is Eulerian or a thickness-
 263 weighted average in buoyancy coordinates. We find that the Eulerian-average approach to
 264 analyzing squeeze dispersion is more cumbersome and more difficult to interpret than the
 265 relatively clear result of the thickness-weighted average approach used in section 3.

266 *Note: We have modified the following paragraph to correct a mistake in the original sub-*
 267 *mission in the formula for κ_e , and connect the formula to our analysis in section 4.*

The squeeze dispersion effective diffusivity in (1) and (9) implies that the bulk dif-
 fusivity of oceanic tracers is estimated by averaging turbulent buoyancy flux and dividing
 by thickness-weighted-average buoyancy gradient. In section 4, we approximate the tur-
 bulent buoyancy flux with $\Gamma\epsilon$, where Γ is the mixing coefficient and ϵ is the turbulent ki-
 netic energy dissipation rate. We then use the instantaneous buoyancy gradient N^2 to es-
 timate the thickness-weighted-average buoyancy gradient $1/\langle 1/N^2 \rangle$, so that the ratio be-
 tween turbulent buoyancy flux and thickness-weighted-average buoyancy gradient expressed
 by (1) and (9) becomes

$$\kappa_e = \left\langle \frac{1}{N^2} \right\rangle \langle \Gamma\epsilon \rangle , \quad (18)$$

268 where the angle brackets again denote an average in density space, or on an isopycnal. The
 269 dependence of the effective squeeze dispersion diffusivity (18) on the average turbulent buoy-
 270 ance flux $\langle \Gamma\epsilon \rangle$ is consistent, for example, with the logic used by Voet et al. (2015) to com-
 271 pare the average in-situ turbulent heat flux with a bulk estimate of heat flux from the tem-
 272 perature distribution in the Samoan passage. In section 4, we develop a technique to coarse-
 273 grain the Samoan passage observations reported in Alford et al. (2013) and Voet et al. (2015)
 274 to evaluate equation (18) and interpret its implications for tracer dispersion.

275 Squeeze dispersion is not shear dispersion: squeeze dispersion is proportional to dif-
 276 fusivity while shear dispersion is inversely proportional to diffusivity. Squeeze dispersion re-
 277 quires velocity gradients parallel to the direction of dispersion, while shear dispersion requires
 278 only a velocity gradient perpendicular to the direction of the tracer dispersion. For exam-
 279 ple, vertical oceanic shear dispersion, which is negligible, is associated with lateral variations
 280 in vertical velocity and has an effect that is inversely proportional to lateral diffusivity. Ver-
 281 tical squeeze dispersion, on the other hand, persists under vanishing lateral diffusivity and
 282 is proportional to the strength of the vertical diffusivity.

283 The effective diffusivity for large-scale tracers in equation (1) and (9) implies that mod-
 284 els that use the local diffusivity but do not fully resolve oceanic strain may underpredict oceanic
 285 tracer dispersion. In other words, the parameterization of diapycnal mixing in coarse res-
 286 olution models should take unresolved squeezing into account.

287 Finally, squeeze dispersion may also be important in other, non-oceanic laminar flows
 288 such as confined low Reynolds number flows. In these cases, the thickness h that appears
 289 in equation (1) and (9) should be interpreted as the separation between material sur-
 290 faces.

291 A Barotropic advection of tracer over bathymetry

Introducing the topographic coordinate $\tilde{z} = z \langle H \rangle / H$, where $\langle H \rangle$ is a constant av-
 erage depth and $\langle \phi \rangle = L^{-1} \int_0^L \phi dx$ is the average of any quantity ϕ over a tracer trajec-
 tory from $x = 0$ to $x = L$, the tracer conservation equation (2) with flow field (3) trans-
 forms into

$$c_t + uc_x = \frac{\langle H \rangle^2 \kappa}{H^2} c_{\tilde{z}\tilde{z}} . \quad (A.1)$$

In a coordinate frame following columns of fluid advected horizontally by the flow $u = U/H$ with transport U , the vertical spread of the tracer is described by the deceptively ordinary equation

$$c_s = \langle \kappa \rangle c_{\tilde{z}\tilde{z}}, \quad (\text{A.2})$$

where $\langle \kappa \rangle$ denotes the average values of κ over a trajectory. In (A.2), s is a time-like trajectory coordinate defined by

$$s(t) \stackrel{\text{def}}{=} \frac{\langle H \rangle^2}{\langle \kappa \rangle U} \int_{t_0}^t \frac{\kappa}{H} dt', \quad (\text{A.3})$$

where $\kappa(x, t)$ and $H(x)$ are evaluated along the column trajectory $x = \xi(t)$, which obeys $\dot{\xi}_t = u(\xi)$. The solution to (A.2) on short trajectories and with the initial condition $c = \delta(\tilde{z} - \tilde{z}_0)\delta(x - x_0)$ is

$$c = \frac{1}{\sqrt{4\pi \langle \kappa \rangle s}} \exp \left[-\frac{(\tilde{z} - \tilde{z}_0)^2}{4 \langle \kappa \rangle s} \right] \delta(x - \xi). \quad (\text{A.4})$$

The solution (A.4) is valid when the tracer concentration is negligible at the boundaries, which holds if the trajectory is short and the initial release point \tilde{z}_0 is sufficiently far from the top or bottom. Evaluating (A.4) at $t = \langle H \rangle L/U$ when the tracer patch reaches $x = L$ yields equation (5).

B Derivation of the tracer circulation equation (9)

To derive the tracer circulation equation (9), we apply the thickness-weighted average defined in (8) to the macroscale tracer equation,

$$c_t + \mathbf{u} \cdot \nabla c = \nabla \cdot (\kappa \nabla c), \quad (\text{B.1})$$

first introduced in equation (7). We introduce the variable $\varsigma \stackrel{\text{def}}{=} 1/b_z$ in this appendix for convenience. ς is related to the thickness $h = g/b_z$ via $\varsigma = h/g$ and corresponds to the variable σ in Young (2012). In terms of ς the thickness-weighted average in (8) is $\hat{\phi} \stackrel{\text{def}}{=} \langle \varsigma \phi \rangle / \langle \varsigma \rangle$ for any variable ϕ .

We first transform the macroscale tracer equation (B.1) from the Cartesian coordinates x, y, z, t to the buoyancy coordinates $\tilde{x}, \tilde{y}, \tilde{b}, \tilde{t}$. A thorough review of buoyancy coordinates is given by Young (2012). The material derivative $D/Dt \stackrel{\text{def}}{=} \mathbf{u} \cdot \nabla c = u\partial_x + v\partial_y + w\partial_z$ in buoyancy coordinates is

$$\frac{D}{Dt} = u\partial_{\tilde{x}} + v\partial_{\tilde{y}} + w\partial_{\tilde{b}}, \quad (\text{B.2})$$

where w is the diabatic contribution to the buoyancy conservation equation such that $Db/Dt = w$. We define w as

$$w \stackrel{\text{def}}{=} \nabla \cdot (\kappa \nabla b), \quad (\text{B.3})$$

consistent with the diabatic contribution to the macroscale tracer equation (B.1). In other words, we use a closure with turbulent diffusivity κ to approximate the effect of microstructure fluxes for all tracers.

We simplify the microscale diabatic term $\nabla \cdot (\kappa \nabla c)$ on the right side of (B.1) with two assumptions. First, we assume that buoyancy surfaces have small slopes and neglect terms proportional to $\zeta_{\tilde{x}}$ or $\zeta_{\tilde{y}}$, where $z = \zeta(\tilde{x}, \tilde{y}, \tilde{b}, \tilde{t})$ is the height of the buoyancy surface \tilde{b} . Second, we assume diffusive isopycnal tracer fluxes on circulation scales are dominated by macroscale stirring rather than microscale turbulence. We thus consider only the diabatic component of the diabatic flux, so that

$$\kappa \nabla c \approx \frac{\kappa C_{\tilde{b}}}{\varsigma^2} \mathbf{e}_3, \quad (\text{B.4})$$

304 where $\mathbf{e}_3 = \mathbf{k}/\varsigma$ is the third covariant buoyancy-coordinate basis vector (Young, 2012) and
 305 \mathbf{i} , \mathbf{j} , and \mathbf{k} are the east, north, and vertical Cartesian coordinate unit vectors. Applying the
 306 same assumptions to the diabatic buoyancy flux implies that $\varpi \approx \varsigma^{-1} \partial_{\tilde{b}} (\kappa/\varsigma)$.

We turn to the thickness-weighted average of the advection term Dc/Dt in (B.1).
 For any variable ϕ , the thickness-weighted decomposition

$$\phi = \hat{\phi} + \phi'' \quad (\text{B.5})$$

defines the perturbation ϕ'' . A key identity derived by Young (2012) is

$$\left\langle \varsigma \frac{Dc}{Dt} \right\rangle = \langle \varsigma \rangle \left(\frac{D^\# \hat{c}}{Dt} + \nabla \cdot \mathbf{J}^c \right), \quad (\text{B.6})$$

where the residual material derivative

$$\frac{D^\#}{Dt} \stackrel{\text{def}}{=} \hat{u}\partial_x + \hat{v}\partial_y + w^\#\partial_z \quad (\text{B.7})$$

describes advection by the residual velocity field $\mathbf{u}^\# = (\hat{u}, \hat{v}, w^\#)$. The meaning of $w^\#$
 is described in the next paragraph. The perturbation flux in (B.6) is

$$\mathbf{J}^c \stackrel{\text{def}}{=} \widehat{u''c''} \langle \mathbf{e}_1 \rangle + \widehat{v''c''} \langle \mathbf{e}_2 \rangle + \widehat{\varpi''c''} \langle \mathbf{e}_3 \rangle \quad (\text{B.8})$$

where the average basis vectors $\langle \mathbf{e}_j \rangle$ are defined

$$\langle \mathbf{e}_1 \rangle \stackrel{\text{def}}{=} \mathbf{i} - \mathbf{k} b_x^\# / b_z^\#, \quad \langle \mathbf{e}_2 \rangle \stackrel{\text{def}}{=} \mathbf{j} - \mathbf{k} b_y^\# / b_z^\#, \quad \langle \mathbf{e}_3 \rangle \stackrel{\text{def}}{=} \mathbf{k} / b_z^\#. \quad (\text{B.9})$$

The vertical velocity $w^\#$ in (B.7) and buoyancy field $b^\#$ in (B.9) are defined in terms
 of the average depth of a buoyancy surface, $\langle \zeta \rangle$. In particular, $b^\#$ is defined via $z = \langle \zeta \rangle (\tilde{x}, \tilde{y}, b^\#, \tilde{t})$
 and is therefore the value of the buoyancy surface whose mean position is x, t . The resid-
 ual vertical velocity $w^\#$, on the other hand, is defined in terms of the motion of $\langle \zeta \rangle$ via

$$w^\# \stackrel{\text{def}}{=} \frac{D^\# \langle \zeta \rangle}{Dt}. \quad (\text{B.10})$$

In this sense, $w^\#$ and $\langle \zeta \rangle$ have a similar relationship as w and ζ . Neither $w^\#$ nor $b^\#$ are
 equal to their thickness-weighted counterparts \hat{w} and \hat{b} .

Turning back to the diabatic contribution on the right of (B.1), we use (B.4) and the
 identity $\langle \varsigma \nabla \cdot \mathbf{F} \rangle = \nabla \cdot \hat{\mathbf{F}}^j \langle \mathbf{e}_j \rangle$ to obtain

$$\widehat{\nabla \cdot (\kappa \nabla c)} = \nabla \cdot \frac{\langle \kappa/\varsigma \rangle \hat{c}_{\tilde{b}} + \langle \kappa c''_{\tilde{b}}/\varsigma \rangle}{\langle \varsigma \rangle} \langle \mathbf{e}_3 \rangle. \quad (\text{B.11})$$

We then use $\varpi = \varsigma^{-1} \partial_{\tilde{b}} (\kappa/\varsigma)$ to combine (B.11) with the divergence of the diapycnal
 term $\widehat{\varpi''c''} \langle \mathbf{e}_3 \rangle$ in (B.8) and transform the part of the result that depends on \hat{c} to Car-
 tesian coordinates. When the dust settles, we find that

$$\nabla \cdot \widehat{(\varpi''c'' - \kappa \nabla c)} \langle \mathbf{e}_3 \rangle = -\partial_z \left(\langle \varsigma \rangle \left\langle \frac{\kappa}{\varsigma} \right\rangle \partial_z \right) \hat{c} + \nabla \cdot \frac{\langle c'' \partial_{\tilde{b}} (\kappa/\varsigma) - \kappa c''_{\tilde{b}}/\varsigma \rangle}{\langle \varsigma \rangle} \langle \mathbf{e}_3 \rangle. \quad (\text{B.12})$$

The first term on the right of (B.12) describes the squeeze dispersion of \hat{c} , while the sec-
 ond term corresponds to the diabatic macroscale perturbation flux associated with the dif-
 ference between the tracer distribution c and buoyancy distribution b .

We use (B.6) and (B.12) to write the thickness-weighted-average of (7):

$$\left(\partial_t + \mathbf{u}^\# \cdot \nabla - \partial_z \kappa_e \partial_z \right) \hat{c} = -\nabla \cdot \mathbf{E}^c, \quad (\text{B.13})$$

where $\kappa_e \stackrel{\text{def}}{=} \langle h \rangle \langle \kappa/h \rangle = \langle s \rangle \langle \kappa/s \rangle$ and

$$\mathbf{E}^c \stackrel{\text{def}}{=} \widehat{u''c''} \langle \mathbf{e}_1 \rangle + \widehat{v''c''} \langle \mathbf{e}_2 \rangle + \langle s \rangle^{-1} \langle c'' \partial_{\tilde{b}} (\kappa/s) - \kappa c''_{\tilde{b}} / s \rangle \langle \mathbf{e}_3 \rangle. \quad (\text{B.14})$$

312 Acknowledgments

The authors acknowledge beneficial conversations with William R. Young, Jennifer MacKinnon, Carl Wunsch, Jim Ledwell, and Trevor MacDougall. GLW was supported by the NOAA Climate and Global Change Postdoctoral Fellowship Program, administered by UCAR's Cooperative Programs for the Advancement of Earth System Sciences. Samoan Passage research was funded by the National Science Foundation under grants OCE-1029268, OCE-1029483 and OCE-1657795. Julia code and notebooks to generate figures 2 and 3 can be found at <https://github.com/glwagner/SqueezeDispersionGRL>.

320 References

- Alford, M. H., Girton, J. B., Voet, G., Carter, G. S., Mickett, J. B., & Klymak, J. M. (2013). Turbulent mixing and hydraulic control of abyssal water in the Samoan Passage. *Geophysical Research Letters*, 40(17), 4668–4674.
- Alford, M. H., & Pinkel, R. (2000). Observations of overturning in the thermocline: The context of ocean mixing. *Journal of Physical Oceanography*, 30(5), 805–832.
- Aris, R. (1956). On the dispersion of a solute in a fluid flowing through a tube. *Proc. R. Soc. Lond. A*, 235(1200), 67–77.
- Davis, R. E. (1994). Diapycnal mixing in the ocean: Equations for large-scale budgets. *Journal of physical oceanography*, 24(4), 777–800.
- De Szoeke, R. A., & Bennett, A. F. (1993). Microstructure fluxes across density surfaces. *Journal of physical oceanography*, 23(10), 2254–2264.
- Gent, P. R., & Mcwilliams, J. C. (1990). Isopycnal mixing in ocean circulation models. *Journal of Physical Oceanography*, 20(1), 150–155.
- Gregg, M. (1998). Estimation and geography of diapycnal mixing in the stratified ocean. *Physical processes in lakes and oceans*, 305–338.
- Kaminski, A. K. (2016). *Linear optimal perturbations and transition to turbulence in strongly-stratified shear flows* (Unpublished doctoral dissertation). University of Cambridge.
- Ledwell, J., Montgomery, E., Polzin, K., Laurent, L. S., Schmitt, R., & Toole, J. (2000). Evidence for enhanced mixing over rough topography in the abyssal ocean. *Nature*, 403(6766), 179.
- Ledwell, J., St. Laurent, L., Girton, J., & Toole, J. (2011). Diapycnal mixing in the Antarctic circumpolar current. *Journal of Physical Oceanography*, 41(1), 241–246.
- Mashayek, A., Ferrari, R., Merrifield, S., Ledwell, J. R., St Laurent, L., & Garabato, A. N. (2017). Topographic enhancement of vertical turbulent mixing in the Southern Ocean. *Nature Communications*, 8, 14197.
- MacDougall, T. J., & McIntosh, P. C. (2001). The temporal-residual-mean velocity. part ii: Isopycnal interpretation and the tracer and momentum equations. *Journal of Physical Oceanography*, 31(5), 1222–1246.
- Oakey, N., & Elliott, J. (1982). Dissipation within the surface mixed layer. *Journal of Physical Oceanography*, 12(2), 171–185.
- Osborn, T. (1980). Estimates of the local rate of vertical diffusion from dissipation measurements. *Journal of Physical Oceanography*, 10(1), 83–89.
- Redi, M. H. (1982). Oceanic isopycnal mixing by coordinate rotation. *Journal of Physical Oceanography*, 12(10), 1154–1158.

- 358 St. Laurent, L., Naveira Garabato, A. C., Ledwell, J. R., Thurnherr, A. M., Toole,
359 J. M., & Watson, A. J. (2012). Turbulence and diapycnal mixing in Drake
360 Passage. *Journal of Physical Oceanography*, 42(12), 2143–2152.
- 361 Voet, G., Girton, J. B., Alford, M. H., Carter, G. S., Klymak, J. M., & Mickett, J. B.
362 (2015). Pathways, volume transport, and mixing of abyssal water in the Samoan
363 Passage. *Journal of Physical Oceanography*, 45(2), 562–588.
- 364 Watson, A. J., Ledwell, J. R., Messias, M.-J., King, B. A., Mackay, N., Meredith,
365 M. P., ... Garabato, A. C. N. (2013). Rapid cross-density ocean mixing at mid-
366 depths in the Drake Passage measured by tracer release. *Nature*, 501(7467),
367 408.
- 368 Young, W. R. (2012). An exact thickness-weighted average formulation of the Boussi-
369 nesq equations. *Journal of Physical Oceanography*, 42(5), 692–707.